Implementation of coded targets for metrology applications in MicMac, a free open-source photogrammetric software

Jean-Michael Muller[1], Mehdi Daakir[1], Marc Pierrot Deseilligny[1], Florian Barcet[2]

[1] Univ. Gustave Eiffel, ENSG, IGN, LASTIG, F-94160 Saint-Mandé, France
[2] CERN, Geneva, Switzerland

Technical Commission II

Keywords: Photogrammetry, Metrology, Coded targets, Simulation, MicMac, Open-source software

Abstract

Image-based metrology is an increasingly utilized technique across a wide range of industrial applications, largely due to its reliance on precisely measurable and automatically detectable patterns within images. In photogrammetry, coded and uncoded targets, such as ground control points, are commonly used throughout the photogrammetric processing chain. This study presents recent developments in the integration of coded-targets within *MicMac*, a free open-source photogrammetric software. These developments were undertaken in collaboration between *IGN* and *CERN* for future accelerator alignments using image-based ecartometric measurement.

One key goal, addressed in this paper, is the creation of a flexible coded-target generator within *MicMac*, allowing users to specify various constraints for target generation. Additionally, detection and simulation tools were implemented and evaluated. This paper focuses on the use of a common circular coded-target pattern, and introduces a novel home-made target design optimized for both image measurements and topometric instruments. Results from 2D and 3D simulations, as well as real data, demonstrate performance similar to commercial software solutions using circular coded-target, or even superior in certain configurations using our home-made target pattern. To our best knowledge, *MicMac* is the only free and open-source software achieving these levels of performance.

1. Introduction

Coded targets is a widely used technique in the field of photogrammetric metrology and machine vision applications (Hurník et al., 2021). It is highly beneficial for several reasons: it enables automated processing of images, high-precision measurements by achieving sub-pixel accuracy and unique identification of detected points across images.

In 2023, *IGN*[1] (National Institute of Geographic and Forest Information - The French Mapping Agency) and *CERN*[2] (European Organization for Nuclear Research) started a scientific collaboration to develop ecartometry tools in the free open-source photogrammetric software *MicMac*[3] (Rupnik et al., 2017) version 2 (also named *MMVII*) maintained at *LASTIG*[4] lab. Ecartometry involves measuring the radial deviation between a stretched wire and a magnet (Mergelkuhl et al., 2018). These measurements are used in the alignment of particle accelerators. The same measurements, when carried out through photogrammetric acquisitions, require tools to perform various tasks: interior orientation, exterior orientation, rigid block calibration, integration of inclinometric measurements, and wire detection (Barcet et al., 2024). These steps involve points materialized by targets that must be detected automatically, accurately, and precisely in the images. The purpose of this article is to present the developments made for coded-targets integration in *MMVII*.

[1] https://www.ign.fr
[2] https://home.cern
[3] https://github.com/micmacIGN
[4] https://www.umr-lastig.fr

2. Automatic Targets

Numerous variations of coded-targets have been developed in computer vision, demonstrating high efficiency for image-based measurement. While this study focuses on two specific target patterns, it is important to mention the broader landscape of coded-target systems used in optical metrology. For example, (Ahn et al., 2001) proposed a target design using only circular elements for the target center, code and background. (Shortis and Seager, 2014) developed a target pattern that is easy to manufacture with a detailed detection algorithm enabling straightforward implementation aiming to provide an alternative to commercial systems. Furthermore, (Liu et al., 2021) proposed a variant of circular coded-target (*CCT*), named concentric-*CCT* (*CCCT*), designed to improve detection performance under low-light conditions and challenging viewing angles.

However, a need for alternative patterns designed for survey measurement by total station and with a higher flexibility for its encoding remains and become essential in many precise metrology contexts. In our study, we focus on a circular coded-target pattern (Schneider, 1991) widely used in commercial solutions. Additionally, we have developed a custom chessboard-type pattern designed to make the target compatible with both image and survey-based measurements. Figure 1 provides an overview of the targets that can be generated using *MMVII*.

These different targets patterns bring the following benefits:

- 1a, 1b and 1d are designed for mixing survey and

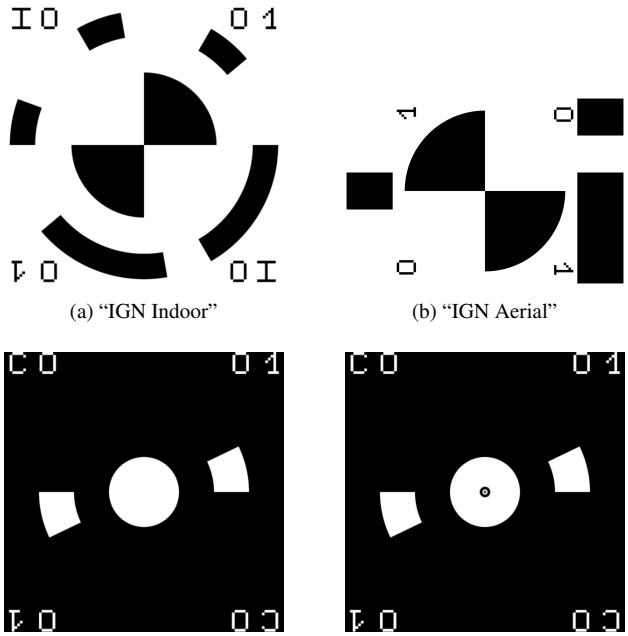

(a) "IGN Indoor" (b) "IGN Aerial"

(c) "Circular" (d) "Circular Topo"

Figure 1: The different coded-target patterns supported by *MMVII*

photogrammetry, being easily readable and aimed at with a reticle of an optical instrument.

- 1c and potentially 1d are compatible with other photogrammetric softwares.
- the global shape of the targets have different proportions to fit the object on which they are placed.
- the pattern shape (radii, width and blank space) is customizable to be able to choose the optimum combination.
- the encoding method (number of code bits, minimal Hamming distance, maximal run length, circular permutations and parity check) is customizable. to adjust the coding to the number of targets needed and avoid decoding errors.

Particular attention was placed on target detection speed and precise target center estimation.

In this paper we will focus on targets types 1a (*MMVII* default) and 1c (circular type, compatible with other photogrammetric software).

2.1 Generation

Once the target type is selected, the next consideration is the choice of encoding method. Encoding refers to a set of bit-vector codes used to uniquely identify targets. Several parameters are essential to define an encoding:

- **Number of (unique) targets**: Determines the total target count achievable.
- **Bit count**: If too few, there won't be enough targets; if too many makes decoding more difficult if image resolution is too low.
- **Robustness against few bits errors**: Measured by Hamming distance, this indicates how resilient the code is to bit errors.
- **Consecutive identical bits**: Minimizing consecutive identical bits can aid in precise target detection (codes alternating bits present higher contrast between bits). Generally referred to as *MRL* : Maximum Run Length.
- **Maximum Number of Targets**: Optimizes target selection from the possible set for a particular encoding.

Considering that codes are identical under a subset S of circular permutation we define the Hamming distance as follow:

$$D_H^S(V_1, V_2) = \min_{s \in S} D_H(V_1, s(V_2))$$

For the circular target type, the encoding is fixed to keep compatibility with existing software. The only choice is the number of bits:

- 12-bit for 147 different targets
- 14-bit for 516 different targets
- 20-bit for 24793 different targets

For our experiments (see Sec. 3), we used circular targets with 14-bit encoding, while "IGN" targets employed an 18-bit encoding with a minimum Hamming distance of 3 bits and maximum run lengths of 2 bits for zeros and 3 bits for ones. This setup ensures a similar number of distinct targets for both types: 516 for the circular targets and 564 for the "IGN" targets.

2.2 Detection

We present below the algorithms implemented in *MMVII* for both circular (see Sec. 2.2.1) and "IGN" targets (see Sec. 2.2.2) detection process.

2.2.1 Circular Targets For this type of targets, the main idea is that locally, image deformation can be approximated by an affine transformation, meaning that a target, initially circular, appears as an ellipse in the image.

The main steps involved in the detection process are the following: 1. detection of the seed points, 2. estimation of radiometric properties and connected component analysis (CCA), 3. estimation of the ellipse parameters and 4. transforming the image into polar coordinates to linearize the code and perform the decoding part.

Seed detection Seed detection is the initial stage of the process where every pixel is analyzed. Assuming the shape is an ellipse (i.e., a convex shape), it has a single point that is maximal in a given direction. Here, we arbitrarily choose the upward-vertical direction and detect these points using a series of criteria:

- The point has a positive y-gradient.
- The x-gradient at the point changes sign.
- Among the points meeting the above criteria, the y-gradient is locally maximal within a neighborhood
- Threshold criteria on contrast value.

Figure 2 shows an example of resulting seed points selected on an image.

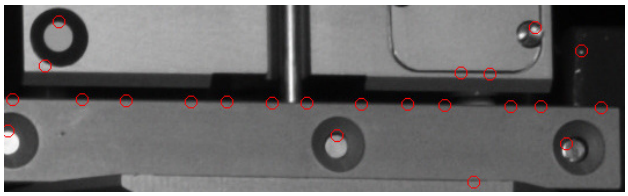

Figure 2: Example of selected seed points

Radiometric modeling and CCA Several assumptions are considered : (i) targets are black and white ; (ii) locally, the image radiometry can be modeled as binary with some blurring and noise ; (iii) black and white regions of the target are radiometrically extreme. We define a first estimation of the ellipse as the connected component where seed points serve as starting points. Figure 3 shows an example of the result obtained at this step.

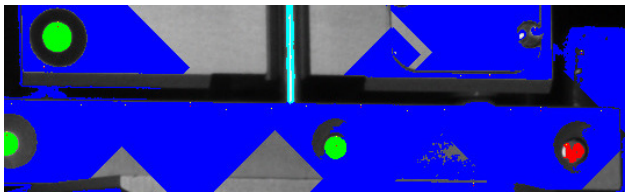

Figure 3: Example of *CCA* result

Ellipse estimation To extract the potential ellipse from the connected component, we follow these steps:

1. **Frontier Extraction**: Identify frontier pixels in the connected component.
2. **Refine Coordinates**: Using the centroid C as an approximate center of the ellipse, refine each frontier point P by finding a point Q along the line $\overrightarrow{CP}$ where intensity $I(Q) = \frac{B+W}{2}$ (a value between black and white), approximated through intensity interpolation.
3. **Ellipse Parameter Estimation**: Using the coordinates of frontier points.

Figure 4 shows the fitted ellipse (Fig. 4a) and a zoomed view of its frontier (Fig. 4b).

After extracting the parameters, the ellipse is validated using two criteria:

- **Distance Test**: Calculate the average distance between frontier points and the fitted ellipse.
- **Gradient Test**: Sample points on the ellipse and compare the theoretical gradient with the gradient in the image.

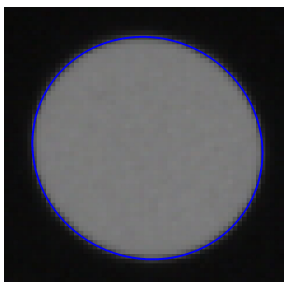

(a) Example of a fitted ellipse

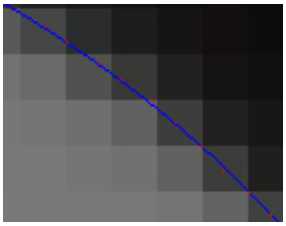

(b) Zoom on points along the ellipse frontier

Figure 4: Result of ellipse estimation

Code extraction Once an ellipse has been determined and validated, in order to extract its code, we proceed to a change of coordinate system, switching to polar coordinates. Figure 5 shows an example of polar image extracted from a target.

Figure 5: Example of target code extraction

For each interval, the bit-code is computed simply by thresholding its values with $\frac{B+W}{2}$.

2.2.2 "IGN" Targets These targets are found and optimized mainly using the chessboard central pattern. The lines intersections are very efficient for center estimation. The method used is designed to be very efficient on small targets.

The main steps are: 1. initial candidate centers detection, 2. finding a small chessboard axes around the center, 3. black and white values estimation, 4. extension of the axes and refining axes and center, 5. finding the two black ellipse quarters, 6. finding the ellipse and the target affinity and 7. decoding.

Figure 6 shows the result of these consecutive steps on a target.

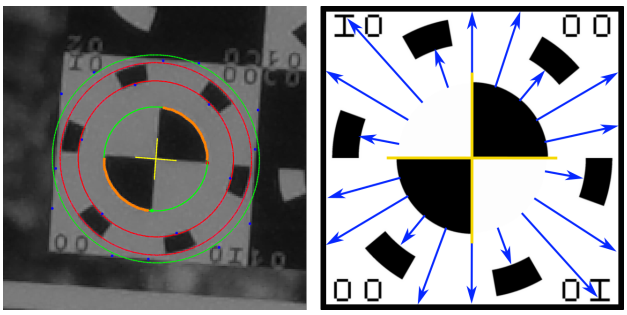

Figure 6: "IGN" target extraction indicators for code `100100100100100100`

Initial centers detection Each pixel in the image is analyzed to identify symmetric neighborhoods, with successive criteria applied to proceed to progressive elimination of candidates. The position of potential candidates is refined by fitting a quadratic function.

Chessboard axes Around the center, and assuming the target is at the minimum size accepted, several directions are tested to find the two directions corresponding to the normals to the image gradients (yellow lines in Figure 6). These gradients have to change direction on each side of the center.

Black and white values In the neighborhood of the center, a statistical estimation is performed to find the black and white reference values for the target.

Axis extension The chessboard axes are extended and affined, orthogonally to the B/W gradients. The target's real size and the refined center are then estimated. Using the gradient straight lines proved to be more efficient than relying on ellipse estimation for small targets.

Black ellipse quarters The two black ellipse quarters are identified by connected extension from the center. The initial approximation of ellipse points is obtained by getting points from the border of the black connected components that are distant from the chessboard axes (orange points in Figure 6).

Affinity The orange points are refined by radial extension to locate the point with an interpolated value equal to $I(Q) = \frac{B+W}{2}$. The ellipse is then estimated using these refined points (in orange), with the constraint that its center is fixed to the value determined during the axis extension step. The intersection points between the ellipse and the chessboard axes (marked in red and green in Figure 6) are used to define the affinity between the target and the image frames.

Decoding The bits centers directions, known in the target frame are transformed into the image frame. For each direction, the first white-to-black gradient encountered after the ellipse (blue points and arrows in Figure 6) determines whether the bit is black (close to the ellipse) or white (further from the ellipse).

3. Performance Evaluation

The performance evaluation was conducted in three contexts with different levels of realism and controlled environments : 2D simulation, 3D simulation and real images.

For each configuration, performance was assessed for both circular and "IGN" targets. "IGN" targets were processed using *MicMac* (*MMVII*), while circular targets are processed using *MMVII*, *DPA Pro* (a commercial software from *HEXAGON* company, formerly *AICON* software) and *CERN*'s custom software (Lapardhaja and Lambrou, 2019).

3.1 Synthetic 2D

The synthetic 2D dataset consists of a pseudo-random distribution of targets, varying in size, squeezing (aspect ratio), image noise levels, gradient intensity (bias, commonly observed with flash photography) and contrast between black and white levels.

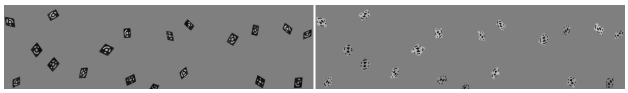

Figure 7: Extract from a synthetic 2D image. Circular targets (left) and "IGN" targets (right).

For each targets settings, four random images, each containing 500 targets were generated. To compare circular targets and "IGN" targets with *MMVII*, images with the same settings and pseudo-random draws were generated, the only difference being the type of target.

Each of the five parameters was studied individually, while keeping all other parameters fixed at their median value. This explains why the outcome of the third parameter combination remains the same across all results tables presented below. Except for the varying parameter, the targets are approximately 40x30 pixels in size, with a noise level of 0.06, a bias of 0.15, and a contrast attenuation of 0.15. Table 1 provides an overview of the parameters with their corresponding value ranges.

Parameter	Interval	Definition
Size (px)	25 - 55	Side of generated target
Ratio	0.4 - 1.0	Ratio between target ellipse axis
Noise	0.0 - 0.1	Amplitude of white noise
Bias	0.0 - 0.3	Amplitude of linear bias
Contrast	0.0 - 0.3	Attenuation of Black/White contrast

Table 1: Simulation parameter ranges

One additional simulation is conducted under ideal conditions: square targets, no noise, no bias, and no contrast attenuation. This additional simulation provides and estimation of the maximum achievable accuracy. Furthermore, we introduce a smaller target size (20 px) in this configuration to evaluate a detection target size threshold.

The detection results are compared to the ground truth provided by the simulation.

3.1.1 Extraction speed All 2D simulations consist of 124 images with a resolution of 24 Mpx each. The full computations for all four software were conducted on the same 10-core computer.

Extraction duration (s)			
DPA Pro Circular Target	CERN Circular Target	MMVII Circular Target	MMVII "IGN" Target
47	546 (mono-thread)	117	172

Table 2: Processing time for 124 images

MMVII is oriented toward precision and flexibility, sometimes at the expense of execution time. Many command-line settings can be changed, making the computation time smaller or much bigger, depending on the minimal target size to look for and precision improvement.

3.1.2 Size variation In this simulation, targets vary in size, from ∼30 to ∼50 pixels for the big side, the aspect ratio being ∼70%. Figure 8 shows the minimum and maximum size values for each target type, while Table 3 presents the corresponding calculation results.

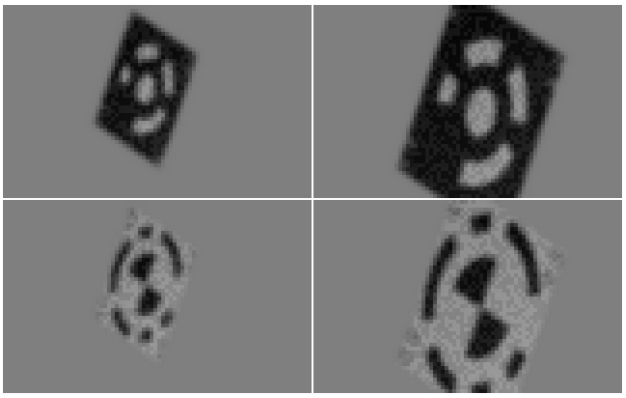

Figure 8: Example of synthetic 2D size variation

	Detected / False decoding (%)			
Target Size (px)	DPA Pro Circular Target	CERN Circular Target	MMVII Circular Target	MMVII "IGN" Target
∼30	34.4 / 0.0	1.5 / 0.3	33.0 / 4.8	95.0 / 0.1
∼35	52.2 / 0.0	8.5 / 0.6	64.5 / 3.5	97.8 / 0.1
∼40	52.4 / 0.0	31.5 / 1.1	86.5 / 0.7	99.2 / 0.0
∼45	51.4 / 0.0	58.1 / 2.6	95.5 / 0.1	99.8 / 0.0
∼50	43.8 / 0.1	79.9 / 2.8	97.7 / 0.0	100.0 / 0.0

(a) 2D simulation detection results for target size variation

	Mean error ± sigma (px)			
Target Size (px)	DPA Pro Circular Target	CERN Circular Target	MMVII Circular Target	MMVII "IGN" Target
∼30	0.06 ± 0.04	0.06 ± 0.04	0.05 ± 0.03	0.06 ± 0.03
∼35	0.07 ± 0.05	0.06 ± 0.03	0.05 ± 0.03	0.06 ± 0.03
∼40	0.06 ± 0.05	0.06 ± 0.04	0.05 ± 0.03	0.05 ± 0.03
∼45	0.05 ± 0.04	0.06 ± 0.04	0.05 ± 0.02	0.05 ± 0.03
∼50	0.05 ± 0.04	0.07 ± 0.04	0.05 ± 0.02	0.05 ± 0.02

(b) 2D simulation center detection results for target size variation

Table 3: 2D simulation results for target size variation, including detection and center accuracy

The results shows that detectability of circular targets is highly sensitive to target size. For reasonable target sizes, *DPA Pro*

detects around 50% of the targets, likely due to image noise (see Table 5a). With "IGN" targets, *MMVII* delivers good results for all tested sizes. False decoding occurs occasionally with *CERN* software, regardless of target size. Similarly, *MMVII* experiences occasional false decoding with circular targets for small targets. Center estimation accuracy is around 0.05 - 0.06 across all sizes and software.

3.1.3 Ratio variation In this simulation, targets vary in aspect ratio. In this case, targets have a large side of ∼40 pixel in length, with the small side ranging between 50% and 90% of the large side. Figure 9 shows the minimum and maximum ratio values for each target type, while Table 4 presents the corresponding calculation results.

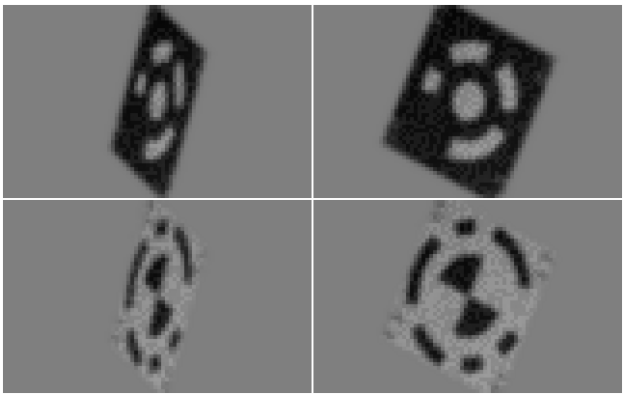

Figure 9: Example of synthetic 2D ratio variation

	Detected / False decoding (%)			
Target Ratio	DPA Pro Circular Target	CERN Circular Target	MMVII Circular Target	MMVII "IGN" Target
∼0.5	33.0 / 0.0	1.9 / 0.1	10.0 / 0.6	88.0 / 0.0
∼0.6	48.4 / 0.0	12.5 / 0.3	47.9 / 1.1	96.8 / 0.0
∼0.7	52.4 / 0.0	31.5 / 1.1	86.5 / 0.7	99.2 / 0.0
∼0.8	52.8 / 0.0	50.9 / 3.5	98.0 / 0.5	99.8 / 0.0
∼0.9	51.7 / 0.0	61.8 / 4.2	99.2 / 0.1	100.0 / 0.0

(a) 2D simulation detection results for target ratio variation

	Mean error ± sigma (px)			
Target Ratio	DPA Pro Circular Target	CERN Circular Target	MMVII Circular Target	MMVII "IGN" Target
∼0.5	0.08 ± 0.05	0.08 ± 0.04	0.05 ± 0.03	0.06 ± 0.03
∼0.6	0.07 ± 0.05	0.07 ± 0.04	0.05 ± 0.03	0.06 ± 0.03
∼0.7	0.06 ± 0.05	0.06 ± 0.04	0.05 ± 0.03	0.05 ± 0.03
∼0.8	0.06 ± 0.05	0.06 ± 0.04	0.05 ± 0.03	0.05 ± 0.02
∼0.9	0.05 ± 0.05	0.07 ± 0.04	0.05 ± 0.02	0.05 ± 0.02

(b) 2D simulation center detection results for target ratio variation

Table 4: 2D simulation results for target ratio, including detection and center accuracy

The results indicate that detection performance depends on target size, especially the smaller side dimension, except for *MMVII* with "IGN" targets. However, the aspect ratio seems to not have a significant impact on center estimation accuracy.

3.1.4 Noise variation In this simulation, image quality is modified by varying the level of noise applied to the image. Figure 10 illustrates the levels of noise introduced on both target type, while Table 5 presents the corresponding calculation results.

The results show that noise is a significant limiting factor for detection using *DPA Pro* and *CERN* software. *MMVII*, particularly with "IGN" targets, seems to be less sensitive to image noise. For all software, the accuracy of center estimation is affected by noise levels.

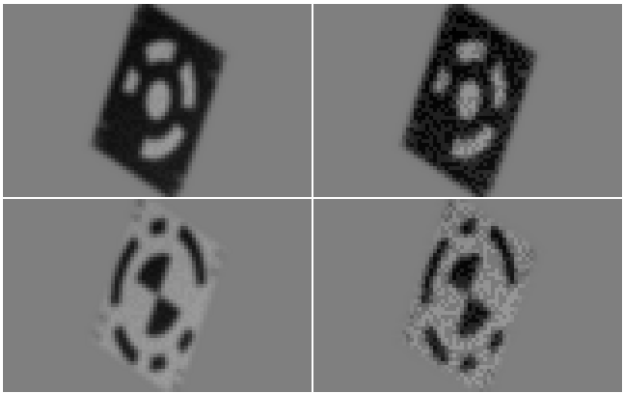

Figure 10: Example of synthetic 2D noise variation

	Detected / False decoding (%)			
Target Noise	DPA Pro Circular Target	CERN Circular Target	MMVII Circular Target	MMVII "IGN" Target
∼0.02	96.5 / 0.0	63.5 / 1.4	97.9 / 0.3	100.0 / 0.0
∼0.04	93.2 / 0.0	49.6 / 1.5	95.5 / 0.7	99.8 / 0.0
∼0.06	52.4 / 0.0	31.5 / 1.1	86.5 / 0.7	99.2 / 0.0
∼0.08	16.2 / 0.0	13.0 / 0.8	57.3 / 1.1	97.7 / 0.0
∼0.10	5.5 / 0.0	3.7 / 0.2	23.3 / 1.4	94.4 / 0.0

(a) 2D simulation detection results for target noise variation

	Mean error ± sigma (px)			
Target Noise	DPA Pro Circular Target	CERN Circular Target	MMVII Circular Target	MMVII "IGN" Target
∼0.02	0.02 ± 0.02	0.05 ± 0.03	0.04 ± 0.01	0.05 ± 0.01
∼0.04	0.04 ± 0.03	0.05 ± 0.03	0.04 ± 0.02	0.05 ± 0.02
∼0.06	0.06 ± 0.05	0.06 ± 0.04	0.05 ± 0.03	0.05 ± 0.03
∼0.08	0.07 ± 0.05	0.08 ± 0.05	0.06 ± 0.03	0.06 ± 0.03
∼0.10	0.09 ± 0.06	0.09 ± 0.06	0.07 ± 0.04	0.07 ± 0.04

(b) 2D simulation center detection results for target noise variation

Table 5: 2D simulation results for target noise variation, including detection and center accuracy

3.1.5 Bias variation In this simulation, the gradient between the dark and clear edges of the targets is varied. Figure 11 shows the impact of the introduced bias for each target type, while Table 6 summarizes the corresponding calculation results.

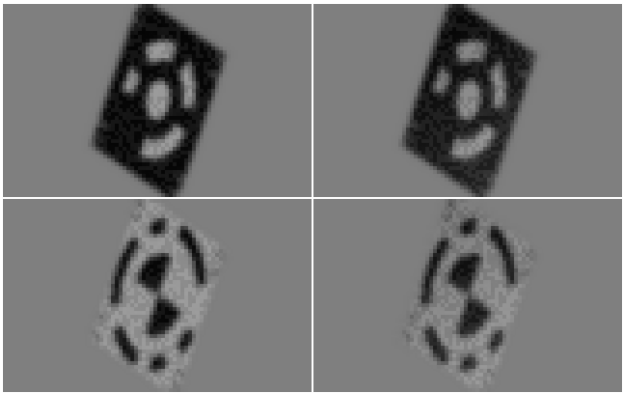

Figure 11: Example of synthetic 2D bias variation

The results show that target gradients affect detection performances for both *CERN* software and *MMVII* with circular targets. For precise center estimation, *MMVII* with "IGN" targets is the most impacted by bias.

3.1.6 Contrast attenuation In this simulation, the contrast between the black and white areas of the targets is varied to simulate different exposure conditions. Figure 12 displays the rendering for the extreme values of the variation range for both types of targets, while Table 7 presents the corresponding

	Detected / False decoding (%)			
Target Bias	DPA Pro Circular Target	CERN Circular Target	MMVII Circular Target	MMVII "IGN" Target
∼0.05	54.6 / 0.0	36.2 / 0.8	90.8 / 0.8	99.4 / 0.0
∼0.10	52.6 / 0.0	34.2 / 1.0	89.0 / 0.8	99.3 / 0.0
∼0.15	52.5 / 0.0	31.5 / 1.1	86.5 / 0.7	99.2 / 0.0
∼0.20	50.9 / 0.0	28.0 / 1.3	83.2 / 0.7	98.8 / 0.0
∼0.25	49.6 / 0.0	24.9 / 1.9	77.4 / 0.8	97.9 / 0.0

(a) 2D simulation detection results for target bias variation

	Mean error ± sigma (px)			
Target Bias	DPA Pro Circular Target	CERN Circular Target	MMVII Circular Target	MMVII "IGN" Target
∼0.05	0.05 ± 0.04	0.06 ± 0.03	0.04 ± 0.02	0.03 ± 0.02
∼0.10	0.06 ± 0.05	0.06 ± 0.04	0.04 ± 0.02	0.04 ± 0.02
∼0.15	0.06 ± 0.05	0.06 ± 0.04	0.05 ± 0.03	0.05 ± 0.03
∼0.20	0.06 ± 0.05	0.07 ± 0.04	0.07 ± 0.03	0.07 ± 0.03
∼0.25	0.06 ± 0.05	0.08 ± 0.05	0.08 ± 0.03	0.09 ± 0.03

(b) 2D simulation center detection results for target bias variation

Table 6: 2D simulation results for target bias variation, including detection and center accuracy

calculation results.

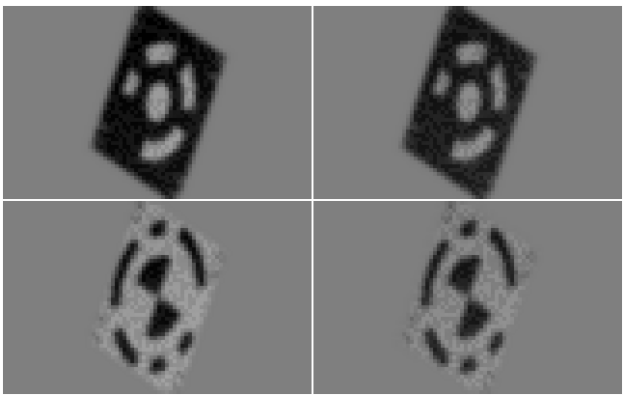

Figure 12: Example of synthetic 2D contrast attenuation variation

	Detected / False decoding (%)			
Target Contrast	DPA Pro Circular Target	CERN Circular Target	MMVII Circular Target	MMVII "IGN" Target
∼0.05	53.2 / 0.0	37.5 / 1.2	90.7 / 0.8	99.5 / 0.0
∼0.10	53.4 / 0.0	34.9 / 1.2	89.0 / 0.8	99.2 / 0.0
∼0.15	52.4 / 0.0	31.5 / 1.1	86.5 / 0.7	99.2 / 0.0
∼0.20	51.8 / 0.0	27.1 / 1.4	83.0 / 0.8	99.0 / 0.0
∼0.25	49.5 / 0.0	24.3 / 1.2	78.1 / 1.0	98.8 / 0.0

(a) 2D simulation detection results for contrast attenuation variation

	Mean error ± sigma (px)			
Target Contrast	DPA Pro Circular Target	CERN Circular Target	MMVII Circular Target	MMVII "IGN" Target
∼0.05	0.05 ± 0.04	0.06 ± 0.04	0.05 ± 0.02	0.05 ± 0.02
∼0.10	0.06 ± 0.05	0.06 ± 0.04	0.05 ± 0.02	0.05 ± 0.02
∼0.15	0.06 ± 0.05	0.06 ± 0.04	0.05 ± 0.03	0.05 ± 0.03
∼0.20	0.06 ± 0.05	0.07 ± 0.04	0.06 ± 0.03	0.06 ± 0.03
∼0.25	0.07 ± 0.05	0.07 ± 0.04	0.06 ± 0.03	0.06 ± 0.03

(b) 2D simulation center detection results for contrast attenuation variation

Table 7: 2D simulation results for target contrast attenuation variation, including detection and center accuracy

The results show that contrast attenuation reduces target detection for *CERN* software and *MMVII* with circular targets, but it has no significant impact on center estimation.

3.1.7 Ideal conditions This simulation was conducted with square targets, free from noise, bias or contrast attenuation. Under these conditions, smaller targets can be detected, which is why a reduced target size of ∼20 pixels was also tested. Figure 13 displays these "ideal" targets, while Table 8 presents the corresponding calculation results.

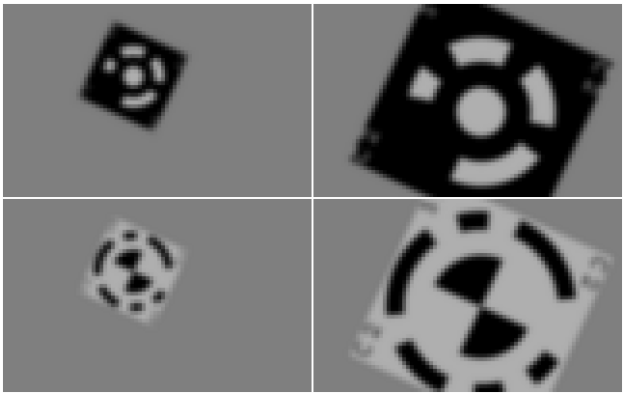

Figure 13: Example of "ideal" synthetic 2D target

	Detected / False decoding (%)			
Target Size (px)	DPA Pro Circular Target	CERN Circular Target	MMVII Circular Target	MMVII "IGN" Target
∼20	7.7 / 0.0	2.0 / 0.2	29.3 / 9.1	98.3 / 0.0
∼30	89.2 / 0.0	54.7 / 0.3	96.0 / 9.7	100.0 / 0.0
∼35	94.5 / 0.0	88.9 / 0.8	99.8 / 0.5	100.0 / 0.0
∼40	99.3 / 0.0	97.9 / 1.1	100.0 / 0.0	100.0 / 0.0
∼45	99.5 / 0.0	98.0 / 1.4	100.0 / 0.0	100.0 / 0.0
∼50	99.7 / 0.0	99.8 / 0.6	100.0 / 0.0	100.0 / 0.0

(a) 2D simulation detection results for "ideal" target

	Mean error ± sigma (px)			
Target Size (px)	DPA Pro Circular Target	CERN Circular Target	MMVII Circular Target	MMVII "IGN" Target
∼20	0.033 ± 0.017	0.035 ± 0.025	0.0014 ± 0.0008	0.0014 ± 0.0008
∼30	0.014 ± 0.009	0.038 ± 0.022	0.0010 ± 0.0006	0.0015 ± 0.0006
∼35	0.010 ± 0.005	0.042 ± 0.024	0.0009 ± 0.0005	0.0016 ± 0.0006
∼40	0.010 ± 0.012	0.043 ± 0.024	0.0009 ± 0.0005	0.0018 ± 0.0006
∼45	0.010 ± 0.011	0.043 ± 0.025	0.0008 ± 0.0005	0.0021 ± 0.0006
∼50	0.010 ± 0.005	0.044 ± 0.025	0.0008 ± 0.0004	0.0023 ± 0.0005

(b) 2D simulation center detection results for "ideal" target

Table 8: 2D simulation results for "ideal" target, including detection and center accuracy

This ideal simulation highlights the sensitivity to noise for circular targets across all tested software. When the target size is sufficiently large, almost all targets are detected. However, false decoding increases significantly for small targets with *MMVII* with circular targets. In contrast, *MMVII* with "IGN" targets gives good performance even with ∼20 pixel size targets. Center estimation is comparable to previous tests for *CERN* software, while it is notably better for other software, especially *DPA Pro* and *MMVII* with circular targets.

3.2 Synthetic 3D

For synthetic 3D images, *Blender*[5], a free and open-source 3D computer graphics software, is used to produce synthetic images of a cube corner equipped with targets. The scene contains 147 targets. Each plan containing 49 regularly placed targets. The simulation is identical for both types of target.

The images have been rendered with a x4 oversampling to minimize aliasing errors. The rendering parameters used in Blender are show in Table 9.

Rendering resolution	400% of 6026 x 4024 pixels
Rendering engine	Cycles
Noise threshold	0.01, max samples 512
Pixel filter	gaussian 1.5 px
Target detection resolution	6026 x 4024 pixels

Table 9: 3D simulation rendering specifications

[5] `https://blender.org`

A virtual camera displacement is used to generate 11 viewpoints with different targets image sizes (from ∼70 to ∼300 pixels). The images represent different viewpoints, resulting in different perspective and lighting conditions. The targets images have a very low noise, but their aspect ratio can be as low as 10%. Figure 14 shows examples of simulated images in a 3D virtual scene.

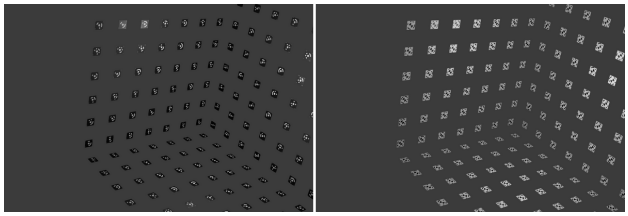

Figure 14: Example of synthetic 3D images

A *Blender* script was developed to export the image coordinates of the target centers for each rendered image. These image coordinates represent the ground truth. Table 10 summarizes the results of this experiment.

Detected / False decoding (%)			
DPA Pro Circular Target	CERN Circular Target	MMVII Circular Target	MMVII "IGN" Target
87.9 / 0.0	89.6 / 0.0	91.5 / 0.0	91.8 / 0.0

(a) 3D simulation detection results

Mean error ± sigma (px)			
DPA Pro Circular Target	CERN Circular Target	MMVII Circular Target	MMVII "IGN" Target
0.029 ± 0.022	0.054 ± 0.044	0.030 ± 0.021	0.004 ± 0.004

(b) 3D simulation center detection results

Table 10: 3D simulation results, including detection and center accuracy

In this case, the detection ratio never reaches 100% because some targets are truncated or excessively flattened. The target center estimation is coherent with the previous tests: noise is low and overall results are satisfactory. *MMVII* with "IGN" targets shows surprisingly good center estimation, certainly due to the low noise, whereas *MMVII* with circular targets is less precise, in contrast with the results obtained in Table 8b.

3.3 Experimental Data

For real data acquisition, a room corner was set up with targets printed on A3 sheets carefully glued. Each plane was equipped with six sheets, each having 24 circular targets and 24 "IGN" targets, resulting in a total of 432 targets per target type across the scene. Each single target represents a 25 mm wide square. Figure 15 illustrates the layout of the scene while Figure 16 shows the layout of the printed targets.

The acquisition consists of 30 images acquired in an arc at different heights. Figure 17 shows the acquisition geometry and Table 11 gives some of the specifications for this experiment. To minimize chromatic aberration and ensure consistency across all software, only the green channel of the raw images was used, forcing all software to process the same single-channel images.

In this configuration, the targets show noise levels comparable to those used in the synthetic 2D images (see Figure 16). The largest side of the targets is about ∼60 pixels with an aspect ratio ranging from ∼30% to ∼100%. Since no theoretical ground truth is available to compare target detection precision, a free bundle adjustment is performed using *MMVII* based on 2D positions of the targets. The comparison is made solely on the residuals of the 2D target positions.

Figure 15: Real case acquisition image example

Figure 16: Real case acquisition targets

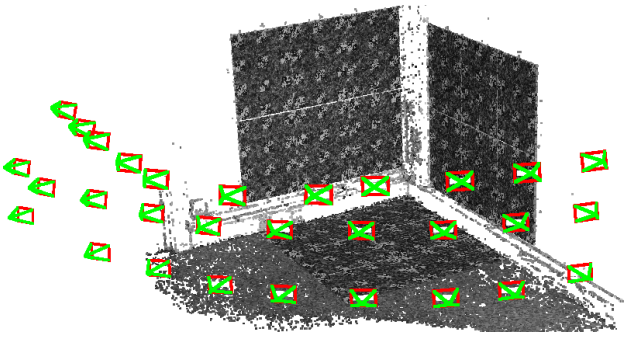

Figure 17: Real-case acquisition geometry

Camera	SONY ILCE-A6400
Sensor size	APS-C (23.5 mm x 15.6 mm)
Sensor resolution	6000 pixels x 4000 pixels
Sensibility	100 ISO
Lens	SAMYANG 24 mm f/1.4 ED AS IF UMC
Mean Distance	∼ 2.5 m

Table 11: Real-case acquisition specifications

In each image, almost all the targets are theoretically visible. Detection performance is comparable to the results of the 2D simulation. *MMVII* with circular targets shows limited efficiency, while with "IGN" targets delivers excellent results. Center accuracy is consistent with 2D simulation results, except for *CERN* software showing irregular results, which explains the wide dispersion value found.

Detected / False decoding (%)			
DPA Pro Circular Target	CERN Circular Target	MMVII Circular Target	MMVII "IGN" Target
67.9 / 0.01	79.0 / 0.02	74.0 / 0.0	98.4 / 0.0

(a) Real-case detection results

Mean error ± sigma (px)			
DPA Pro Circular Target	CERN Circular Target	MMVII Circular Target	MMVII "IGN" Target
0.050 ± 0.033	0.076 ± 0.149	0.036 ± 0.024	0.043 ± 0.027

(b) Real-case center detection results

Table 12: Real-case results, including detection and center accuracy

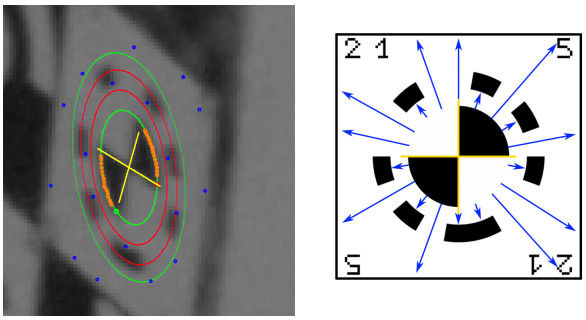

Figure 18: Real-case target decoding error

4. Conclusions

This work concerns the integration and evaluation of tools for detecting coded-targets in images. The primary aim is to provide the scientific community with a free, open-source tool that can be used for image-based metrology with performance levels similar to commercial tools. *MMVII* coded-targets implementation aims to offer the user considerable freedom in the design and parametrization of targets. Users are also provided with detection and simulation tools to evaluate the performance of their settings.

In this article, we focused on two types of patterns: the circular coded-target commonly used in commercial solutions, and a modified pattern which has the advantage of being suitable for both image and topometric measurements.

The performance of these two types of targets was evaluated in three different software, *DPA Pro*, *CERN*'s software and *MMVII*, and by exploring three types of data: simulated data in both 2D and 3D, and real data. The tests show that the performance of target detection and center estimation is affected by several factors such as: target size, noise level, bias, and contrast. Circular targets shows a higher sensitivity to variation of these parameters with unsatisfactory results under challenging conditions. In contrast, "IGN" targets processed with *MMVII* show a consistent performance across all all tested configurations. Center estimation accuracy remained relatively stable in most cases with an average precision of around 0.05–0.06 pixels.

5. Perspectives

Many additional tests could be conducted to improve the internal geometry of "IGN" target pattern. This task can be automated using *MMVII*'s 2D simulation tool, which offers access to many parameters to generate images comparable to real ones. Another promising perspective is improving target detection and decoding methods to handle the case of slightly blurred images. For instance, Figure 18 illustrates difficulty to correctly estimate the chessboard orientation due to blur,resulting in decoding error.

As *MMVII* is still under development and continues to evolve, many significant improvements are anticipated.

Acknowledgment

We would like to acknowledge the financial support provided by *IGN*, *CERN*, and the project *23IND08 DI-Vision* which has received funding from the European Partnership on Metrology, co-financed from the European Union's Horizon Europe Research and Innovation Program and by the Participating States.

References

Ahn, S. J., Rauh, W., Kim, S. I., 2001. Circular coded target for automation of optical 3D-measurement and camera calibration. *International Journal of Pattern Recognition and Artificial Intelligence*, 15(06), 905–919.

Barcet, F., Bestmann, P., Mergelkuhl, D., 2024. Direct Wire Offset Measurements by Photogrammetry Including Gravity Link. *Proceedings of the 17th International Workshop on Accelerator Alignment (IWAA)*.

Hurník, J., Zatočilová, A., Paloušek, D., 2021. Circular coded target system for industrial applications. *Machine Vision and Applications*, 32(1), 39.

Lapardhaja, S., Lambrou, E., 2019. Position determination of encoded and uncoded targets on the large hadron collider at CERN. *Applied Geomatics*, 11(4), 429–437.

Liu, Y., Su, X., Guo, X., Suo, T., Yu, Q., 2021. A novel concentric circular coded target, and its positioning and identifying method for vision measurement under challenging conditions. *Sensors*, 21(3), 855.

Mergelkuhl, D., Vendeuvre, C., Lapardhaja, S., 2018. Recent developments for a photogrammetric system to measure offsets to stretched wires at CERN. *Proceedings of the 15th International Workshop on Accelerator Alignment (IWAA)*.

Rupnik, E., Daakir, M., Pierrot Deseilligny, M., 2017. MicMac–a free, open-source solution for photogrammetry. *Open geospatial data, software and standards*, 2, 1–9.

Schneider, C., 1991. 3-D vermessung von oberflächen und bauteilen durch photogrammetrie und bildverarbeitung. *Proceedings of the IDENT/VISION*, 91, 14–17.

Shortis, M. R., Seager, J. W., 2014. A practical target recognition system for close range photogrammetry. *The Photogrammetric Record*, 29(147), 337–355.